Phase-field study of grain boundary tracking behavior in crack-seal microstructures

Kumar Ankit, Britta Nestler, Michael Selzer, Mathias Reichardt

Karlsruhe Institute of Technology (KIT), IAM-ZBS,
Haid-und-Neu-Str. 7, D-76131, Karlsruhe, Germany

November 4, 2013

Abstract

In order to address the growth of crystals in veins, a multiphase-field model is used to capture the dynamics of crystals precipitating from a super-saturated solution. To gain a detailed understanding of the polycrystal growth phenomena in veins, we investigate the influence of various boundary conditions on crystal growth. In particular, we analyze the formation of vein microstructures resulting from the free growth of crystals as well as crack-sealing processes. We define the crystal symmetry by considering the anisotropy in surface energy to simulate crystals with flat facets and sharp corners. The resulting growth competition of crystals with different orientations is studied to deduce a consistent orientation selection rule in the free-growth regime. Using crack-sealing simulations, we correlate the grain boundary tracking behavior depending on the relative rate of crack opening, opening trajectory, initial grain size and wall roughness. Further, we illustrate how these parameters induce the microstructural transition between blocky (crystals growing anisotropically) to fibrous morphology (isotropic) and formation of grain boundaries. The phase-field simulations of crystals in the free-growth regime (in 2D and 3D) indicate that the growth or consumption of a crystal is dependent on the orientation difference with neighboring crystals. The crack-sealing simulation results (in 2D and 3D) reveal that crystals grow isotropically and grain boundaries track the opening trajectory if the wall roughness is high, opening increments are small and crystals touch the wall before the next crack increment starts. Further, we find that within the complete crack-seal regime, anisotropy in surface energy results in the formation of curved/oscillating grain boundaries (instead of straight) when the crack opening velocity is increased and wall roughness is not sufficiently high. Additionally, the overall capability of phase-field method to simulate large-scale polycrystal growth in veins (in 3D) is demonstrated enumerating the main advantages of adopting the novel approach.

1 Introduction

Veins are sub-planar discontinuities in the earth's crust, containing minerals which precipitate from a super-saturated solution in a fracture (Urai et al., 1991). They exhibit a wide range of crystal habits from dendritic, acicular to crystalline or fibrous structures depending on the boundary conditions (Durney and Ramsay, 1973; Ramsay and Huber, 1983; Fisher and Brantley, 1992; Bons and Jessell, 1997). Hilgers and Urai (2002b) provide an extensive list of such boundary condition: relative rate of crystal growth

Accepted in Contributions to Mineralogy and Petrology
Corresponding Author: kumar.ankit@hs-karlsruhe.de

with respect to fracture opening velocity, degree of crack surface roughness, fluid properties (pressure, temperature, flow velocity and supersaturation) (Cox et al., 1987; Knipe and McCaig, 1994) or transport mechanisms (diffusion and advection) (Durney, 1976; McCaig, 1988; Yardley and Jamtveit, 1997). Durney (1972) and Durney (1976) also correlate fibrous veins to pressure solution and diffusion. The morphology of crystals growing in freely flowing fluid differs significantly from the crystals growing in a constrained environment such as present in crack-sealing conditions. Among the numerous distinguishable crystal morphologies that develop due to a combination of boundary conditions, an interesting case is the formation of curved crystals in veins. Durney and Ramsay (1973) propose that syntectonic fibres grow along the opening trajectory of fracture walls with the transport mechanism being diffusion into the dilational sites. The crystal growth is assumed to be continuous because of which growth competition is not observed. As an alternative to diffusional and continuous accretion, Ramsay (1980) discusses the discontinuous crack-seal mechanism, a repeated process of crack opening and sealing, as indicated by the characteristic inclusion bands/trails and stair-stepped grain boundaries. In recent papers based on natural microstructural features, laboratory experiments and theoretical modeling (Fisher and Brantley, 1992; Bons and Jessell, 1997), it is suggested that crystal fibers in veins can only form by a diffusional accretion process.

Williams and Urai (1989) elucidate that the primary reason responsible for such deviations from the equilibrium crystal shape is mechanical coupling of wall rock and evolving crystals. Further, Hilgers and Urai (2002b) amend that mechanical coupling of vein and wall is not a necessary condition for the formation of curved fibrous crystals, if the crack increments are smaller than about 10 μm.

Cox and Etheridge (1983) and Urai et al. (1991) propose a kinematic model for crystal growth in crack seal veins and show the importance of the wall-rock morphology for the resulting vein microstructure. According to this model, if the crystals have already sealed the space available before the next crack event, the facets are lost and they assume the morphology of the rough vein wall interface. If opening increments are sufficiently small, the crystals cannot develop crystal facets and therefore, grow isotropically. An important conclusion of this model is that the crystal growth kinetics is effectively isotropic if the crack surface is sufficiently rough and crack opening rate is smaller as compared to rate of crystal growth front. As a step to implement crystal anisotropy in 2D, an efficient numerical program *Vein Growth* is developed by Bons (2001) which is further utilized to simulate the anisotropic growth of crystals under complex boundary conditions. Simulations with *Vein Growth* produce fibrous crystals with the potential to track the opening trajectory of the crack when the wall morphology is rough and the average opening velocity is smaller than the growth velocity of the crystals (Koehn et al., 2000; Hilgers et al., 2001). A 2D simulation program FACET is separately developed by Zhang and Adams (2002) to study the growth of polycrystal based on deposition flux of atoms. Nollet et al. (2006) use the algorithms *Vein Growth* and FACET to study crystal growth competition leading to orientation selection and transition from blocky to fibrous morphology during crack-seal growth.

The numerical programs *Vein Growth* and FACET suffer from geometric restrictions and are vulnerable to inaccuracies at triple/quadruple crystal junctions. The artifacts of the algorithm *Vein Growth* namely 'Crystal terminations' and 'Long-distance effects' cause the euhedral angles between facets at crystal terminations to depart from an angle corresponding to the equilibrium shape and the effect of non-neighboring crystals on growth process respectively. Further, the method advocates the switching of the numerical program to FACET in order to produce *crystallographically correct* facets that develop during free growth of crystals. However, the switching of numerical program induces new complications; the complete sealing of the crack can no longer be simulated correctly. Besides, the algorithm FACET is not capable of generating the crystal facets from a randomly shaped nucleus and implicitly assumes the presence of *crystallographically correct* facets prior to the growth process. These aspects are addressed in great detail by Nollet et al. (2005). We recognise that since neither of the methods used in the past are

able to completely describe the crystal growth in veins and restricted to two dimensions, it is important to develop better algorithms to enhance the knowledge concerning the vein growth process.

The phase-field method, long established in the material science community, is a stand-out approach to describe microstructural evolution during phase transitions for e.g. solidification, spinodal decomposition etc. (Chen, 2002; Thornton et al., 2003; Singer-Loginova and Singer, 2008; Nestler and Choudhury, 2011) The phase-field method's popularity in modeling material processes is due to the elegance with which it treats moving boundary problems by obviating the necessity to explicitly track the interfaces. Thus it can overcome many of the problems suffered by earlier models such as the *Vein Growth* and FACET. The model equations are derived on the basis of general thermodynamic and kinetic principles and contain a number of phenomenological parameters related to the physical properties of the material. These parameters are determined based on experimental and theoretical information. Different thermodynamic driving forces for microstructure evolution, such as chemical bulk free energy, interfacial energy, elastic strain energy and different transport processes, such as mass diffusion and advection, can be coupled and the effect on the over all evolution process can be studied simultaneously.

In the present article, we use a thermodynamically consistent multiphase-field model (Stinner et al., 2004; Nestler et al., 2005) to extend the 2D numerical studies of vein growth to 3D. We present the specific formulation of the multiphase-field model for crystal growth by considering anisotropy of the surface energy to produce flat facets and sharp corners (Stinner et al., 2004; Nestler et al., 2005). We also briefly discuss about the computational optimization technique used to make large-scale studies feasible in the present simulations. The phase-field model is used to simulate and analyze the kinematic properties of the anisotropic growth competition in polycrystal, arising due to mis-orientation with respect to most preferred growth direction. In this regard, we also make a strict check for any model artifacts (if present). Further, we modify the boundary condition and parameters to present a systematic study of crack-sealing, e.g. crack surface roughness, crack opening velocity, opening trajectory and number of crystal nuclei. Finally, we present a detailed discussion of 2D and 3D phase-field simulation results, benefits of using the new approach and possible extensions of the current numerical model.

2 Phase-field model

We consider a set of phase-field parameters, denoted by $\boldsymbol{\phi}\left(\vec{x},t\right) = \left(\phi_1\left(\vec{x},t\right)\cdots\phi_N\left(\vec{x},t\right)\right)$ where each component of the vector $\phi_\alpha\left(\vec{x},t\right)$ varies smoothly from 1 inside 0 outside the crystal α over a small finite distance ε (diffuse interface). The location of the crystal-liquid or crystal-crystal interface is defined by a level set at $\phi_\alpha\left(\vec{x},t\right) = 0.5$ which is determined mathematically by solving the evolution equation. The external fields like temperature or concentration can be coupled to the phase-field parameter $\boldsymbol{\phi}$, hence no external boundary conditions needs to be applied at the interfaces.

In this article, we use the phase-field equations derived from non-equilibrium thermodynamics guaranteeing a locally positive entropy production. The model is well suited to describe a polycrystalline system by accounting for an arbitrary number of phase-field parameters (Nestler et al., 2005). In the considered applications to crystal growth in veins, we restrict model definition to an isothermal problem. The Helmholtz free energy functional can be formulated as

$$\mathcal{F}\left(\boldsymbol{\phi}\right) = \int_\Omega \left(f\left(\boldsymbol{\phi}\right) + \varepsilon a\left(\boldsymbol{\phi},\nabla\boldsymbol{\phi}\right) + \frac{1}{\varepsilon} w\left(\boldsymbol{\phi}\right)\right) dx, \tag{1}$$

where $f\left(\boldsymbol{\phi}\right)$ is the bulk free energy density, ε is the small length scale parameter related to the interface

width, $a(\boldsymbol{\phi}, \nabla\boldsymbol{\phi})$ is a gradient type and $w(\boldsymbol{\phi})$, a potential type energy density. We discuss each of these terms in detail.

The phase-field parameter $\boldsymbol{\phi}(\vec{x}, t) = (\phi_1(\vec{x}, t) \cdots \phi_N(\vec{x}, t))$ describes the location of 'N' crystals with different orientation. The value of each phase field paramter ϕ_α lies in the interval $[0, 1]$ and fulfils the constraint $\sum_{\alpha=1}^{N} \phi_\alpha = 1$. The integral shown in functional (1) extends over the entire domain of consideration.

The gradient energy density $a(\boldsymbol{\phi}, \nabla\boldsymbol{\phi})$ is given by

$$a(\boldsymbol{\phi}, \nabla\boldsymbol{\phi}) = \sum_{\substack{\alpha,\beta=1 \\ (\alpha<\beta)}}^{N,N} \gamma_{\alpha\beta} a_{\alpha\beta}^2(\boldsymbol{\phi}, \nabla\boldsymbol{\phi}) |\vec{q}_{\alpha\beta}|^2 \tag{2}$$

where $a_{\alpha\beta}(\boldsymbol{\phi}, \nabla\boldsymbol{\phi})$ defines the form of the surface energy anisotropy of the evolving phase boundary and $\gamma_{\alpha\beta}$ is the surface free energy per unit area of the $\alpha - \beta$ boundary which may additionally depend on the relative orientation of the interface. The vector quantity $\vec{q}_{\alpha\beta} = \phi_\alpha \nabla\phi_\beta - \phi_\beta \nabla\phi_\alpha$ is a generalized gradient vector normal to the $\alpha - \beta$ interface. To assign an isotropic surface energy to the $\alpha - \beta$ phase boundary, $a_{\alpha\beta} = 1$ is chosen. For including a strongly anisotropic surface energy, so that crystals develop flat facets and sharp corners according to directions of the crystal symmetry, a piecewise defined function is used

$$a_{\alpha\beta}(\boldsymbol{\phi}, \nabla\boldsymbol{\phi}) = \max_{1 \le k \le \eta_{\alpha\beta}} \left\{ \frac{\vec{q}_{\alpha\beta}}{|\vec{q}_{\alpha\beta}|} \cdot \vec{\eta_{\alpha\beta}} \right\} \tag{3}$$

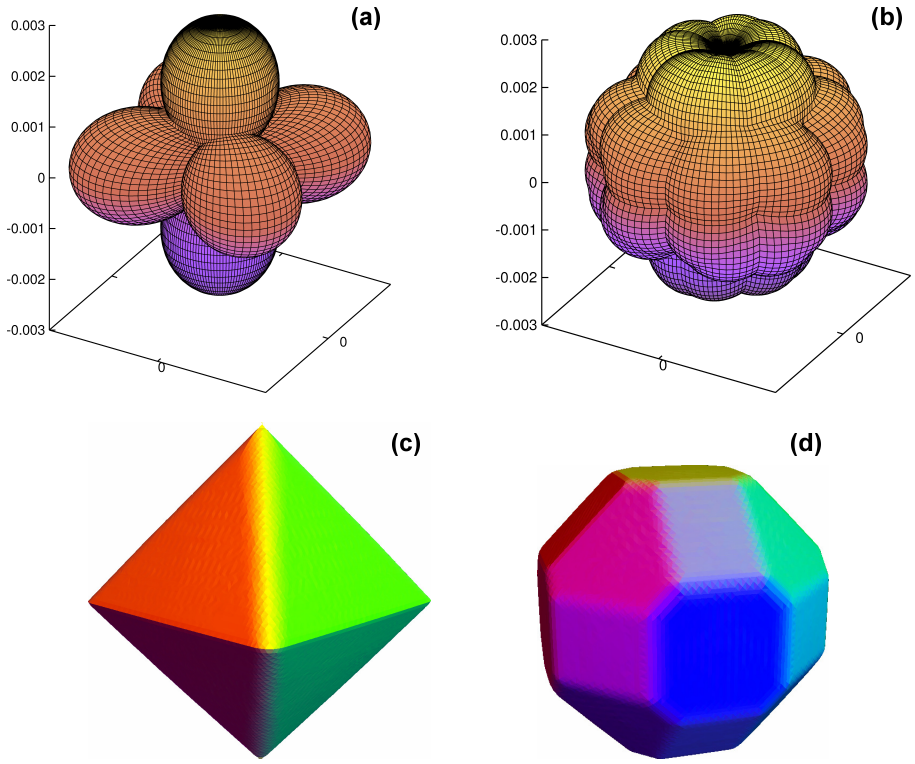

Fig. 1 Polar plot of function (3) for (a) cubic and (b) alum (truncated octahedral symmetry). These anisotropic functions are incorporated in phase-field model to simulate the equilibrium crystal shapes for (c) an octahedral crystal and (d) an alum in free growth conditions. The colors in Figs. 1(c) and 1(d) differentiate among crystal facets.

where $\{\vec{\eta}_{k,\alpha\beta}|k = 1, \cdots, \eta_{\alpha\beta}\}$ for $\eta_{\alpha\beta} \in M$ denotes the complete set of vertex vectors of the corresponding Wulff shape of a crystal α embedded in the bulk phase β and M represents the number of edges. In Figs. 1(a) and 1(b), a polar plot of function (3) for a cubic symmetry and for a truncated octahedral shape are shown. The corresponding equilibrium crystal shapes are displayed in Figs. 1(c) and 1(d), respectively.

In the free energy functional (1), we choose the function $w(\boldsymbol{\phi})$ to represent a multi-obstacle potential in the form of

$$w(\boldsymbol{\phi}) = \begin{cases} \dfrac{16}{\pi^2} \displaystyle\sum_{\substack{\alpha,\beta=1 \\ (\alpha<\beta)}}^{N,N} \gamma_{\alpha\beta}\phi_\alpha\phi_\beta + \sum_{\substack{\alpha,\beta,\delta=1 \\ (\alpha<\beta<\delta)}}^{N,N,N} \gamma_{\alpha\beta\delta}\phi_\alpha\phi_\beta\phi_\delta & \text{if} \quad \boldsymbol{\phi} \in \sum \\ \infty & \text{elsewhere} \end{cases} \tag{4}$$

where $\sum = \left\{\boldsymbol{\phi} \mid \sum_{\alpha=1}^{N} \phi_\alpha = 1 \text{ and } \phi_\alpha \geq 0\right\}$. The higher order term proportional to $\phi_\alpha\phi_\beta\phi_\delta$ in function (4) is added to reduce the presence of an unwanted third or higher-order phase at binary interfaces.

The term $f(\boldsymbol{\phi})$ represents the interface driving force due to the occurrence of different bulk phases. A general formulation of $f(\boldsymbol{\phi})$ can be given as an interpolation of different free energy densities f_α of the bulk phases,

$$f(\boldsymbol{\phi}) = \sum_\alpha f_\alpha h(\phi_\alpha) \tag{5}$$

For studying the kinematics of crystal growth, we apply the interpolation function $h(\phi_\alpha) = \phi_\alpha^3\left(6\phi_\alpha^2 - 15\phi_\alpha + 10\right)$ as a suitable interpolaton function and a constant value for f_α for the bulk free energies.

The evolution equations for the phase fields can be derived from the free energy functional (1) by relating the temporal change of the order parameter, i.e. $\dfrac{\partial\phi_\alpha}{\partial t}$ to the variational derivative of the functional $\mathcal{F}$. Applying the Euler Lagrange formalism yields:

$$\tau\varepsilon\frac{\partial\phi_\alpha}{\partial t} = \varepsilon\left(\nabla \cdot a_{,\nabla\phi_\alpha}(\boldsymbol{\phi}, \nabla\boldsymbol{\phi}) - a_{,\phi_\alpha}(\boldsymbol{\phi}, \nabla\boldsymbol{\phi})\right) - \frac{1}{\varepsilon}w_{,\phi_\alpha}(\boldsymbol{\phi}) - f_{,\phi_\alpha}(\boldsymbol{\phi}) - \lambda \tag{6}$$

$$\lambda = \frac{1}{N}\sum_\alpha \varepsilon\left(\nabla \cdot a_{,\nabla\phi_\alpha}(\boldsymbol{\phi}, \nabla\boldsymbol{\phi}) - a_{,\phi_\alpha}(\boldsymbol{\phi}, \nabla\boldsymbol{\phi})\right) - \frac{1}{\varepsilon}w_{,\phi_\alpha}(\boldsymbol{\phi}) - f_{,\phi_\alpha}(\boldsymbol{\phi}) \tag{7}$$

where the comma separated subindices represent derivatives with respect to ϕ_α and gradient components $\dfrac{\partial\phi_\alpha}{\partial\chi_i}$. The lagrange multiplier λ guarantees the summation constraint $\left(\displaystyle\sum_{\alpha=1}^{N} \phi_\alpha = 1\right)$. In the evolution equation (6), τ is the kinetic coefficient which establishes a relationship between the interface growth

velocity and the driving force. In the following sections, we assume negligible interface kinetic effect and choose the value of τ accordingly. This assumption ensures that the rate at which a nuclei evolves into its equilibrium shape (fast or slow growth mode), is not influenced by interface kinetics.

The phase-field evolution equation (6) is solved numerically using an explicit forward Euler scheme. The spatial derivatives of the right hand side equation are discretized using a second order accurate scheme with a combination of forward and backward finite differences. The phase-field solver is written in programming language C and only solves the evolution equation next to the locally present interfaces. The implementation of such a locally reduced order parameter optimization (LROP) facilitates a reduction in computation time from $O(N^3)$ to $O(1)$ and in memory consumption from $O(N)$ to $O(1)$ per cell in the domain, N being the number of crystals in the system. Thus, the computation is independent of the number of phases making the large scale crystal growth studies feasible even in 3D (Kim et al., 2006; Nestler et al., 2008). Further, the simulation code is highly parallelized on the basis of message passing interface (MPI) standard including 3D domain decomposition and dynamic redistribution schemes. For the present article, the simulations are performed on multiprocessor workstations as well as on a Linux high performance cluster.

3 Free growth in an open cavity

The dependence of growth rate on facet orientations for a single crystal has been reported in the past (Mügge, 1925; Mullin, 2001). However, when polycrystal growth occurs, the neighboring crystals influence the growth rate. Microstructures formed due to crystal growth in an open cavity are characterized by an increase in grain size with more favorably oriented facets out-growing the poorly oriented neighbors (Schmidegg, 1928; Thijssen et al., 1992). The orientation selection rule responsible for the growth competition in such systems is based on mis-orientation with respect to the most preferred growth direction. In the following section, we simulate grain growth competition in 2D and 3D and deduce the orientation selection rule. Since the scope of the current study is limited to kinematics of crystal growth, the driving force is assumed to be constant.

One common mineral analogue that has been used to replicate free growth of crystals in laboratory experiments is Potash alum $[\mathrm{KAl\,(SO_4)_2\cdot 12H_2O}]$ (Nollet et al., 2006). The crystal structure of alum is cubic with eight $\{111\}$ facets. At room temperature it grows into an octahedral habit and also develops $\{110\}$ and $\{100\}$ facets. However, the growth rate of the $\{110\}$ and $\{100\}$ facets is much higher as compared to $\{111\}$, hence they are much smaller in size as compared to the primary facet (Bhat et al., 1992). Klapper et al. (2002) report that temperature fluctuation increases the growth rate of $\{110\}$ and $\{100\}$ facets with respect to $\{111\}$. They also state that crystal dissolution and recrystallization can lead to formation of extra facets in the early growth stages. In the present work, we limit the discussion to cubic symmetry since the kinetics of precipitation of crystals from its salt solution is yet to be incorporated in the present phase-field model.

In the first set of simulations, we study the effect of non-neighboring members (termed as "Long distance effect" by Nollet et al. (2005)) on the free-growth regime of cubic crystals. A 2D simulation is carried out with 10 crystal seeds uniformly embedded at the bottom of the simulation domain and orientation designated as A, B or C degrees. In Fig. 2, the second grain from left at the bottom grain boundary is assigned 'A' degrees and sixth grain as 'B' degrees. All other grains are assigned 'C' degrees. The orientation definitions in 2D simulations are given by Fig. 2(h). Similarly, we simulate the free-growth in 3D by embedding 36 crystal seeds uniformly at the bottom and assigning each orientation A and B once in the domain. The rest of the grains are assigned with orientation value C as shown in Fig. 3. The

numeric value of ‘A’, ‘B’ and ‘C’ are chosen to investigate the effect of non-neighboring crystals (if any) on orientation selection during free-growth of crystals.

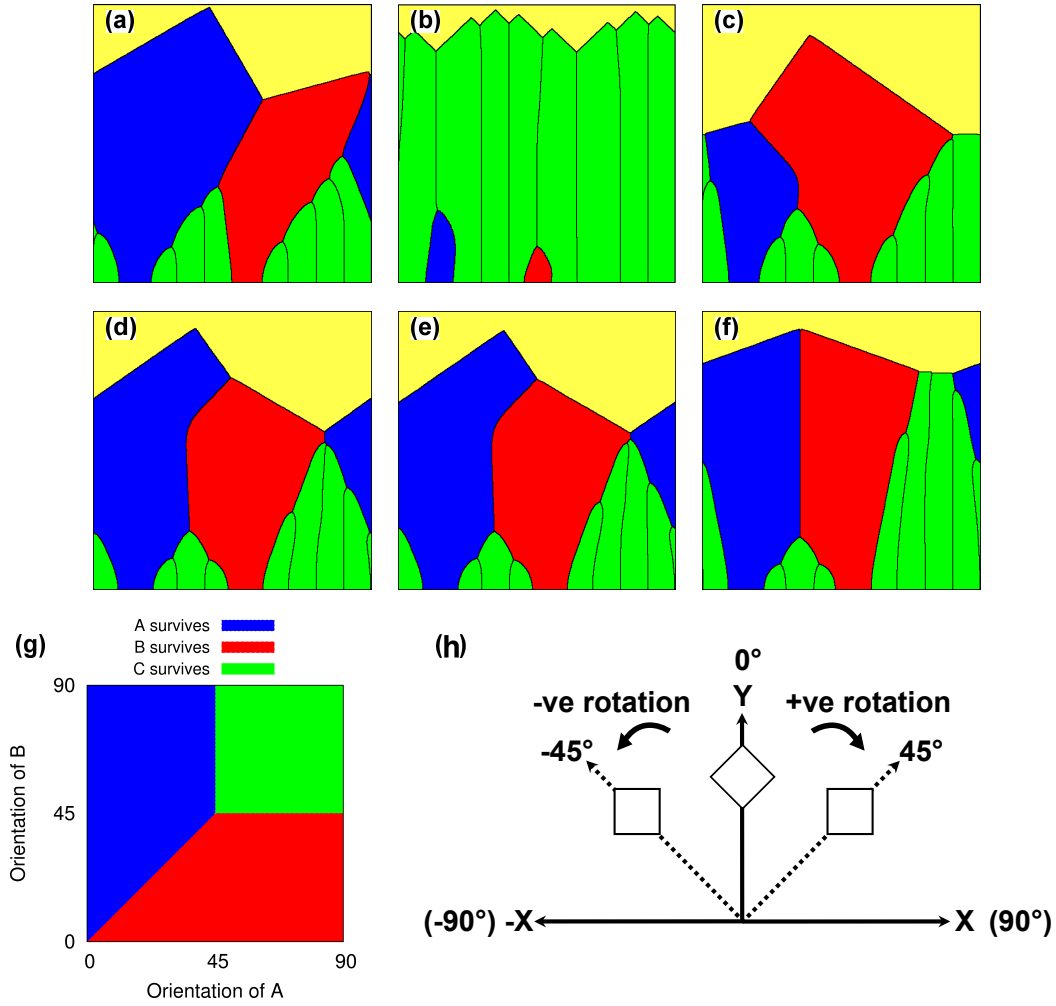

Fig. 2 Anisotropic growth competition of crystals with orientation A (blue), B (red) and C (green). (a) A = 15°, B = 30° and C = 45° (b) A = 15°, B = 30° and C = 0° (c) A = 30°, B = -5° and C = 45° (d) A = 10°, B = -15°and C = 45° (e) A = 11°, B = -15°and C = 45° (f) A = 25°, B = -25° and C =45° (g) Orientation map for C = 45°derived from phase-field simulation results (h) Orientation definition for 2D cubic crystal growth simulations.

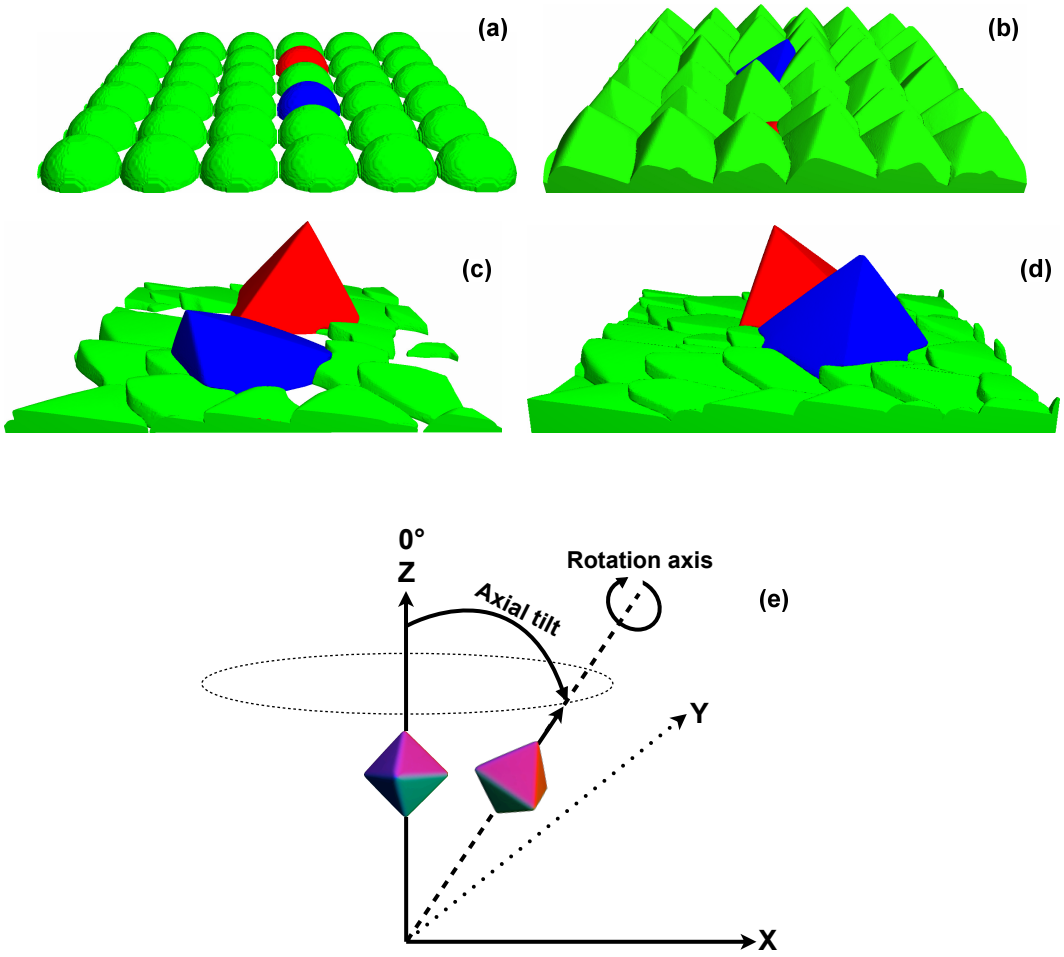

Fig. 3 3D phase-field simulation of cubic crystal growth: (a) Initial condition with hemispherical nuclei uniformly embedded at the bottom of the domain and with assigned orientations of A (blue), B (red) and C (green) degrees. Growth competition leads to orientation selections according to the orientations (b) A = 15°, B = 30° and C = 0° (c) A = 5°, B = 30°and C = 45° (d) A = 15°, B = 10° and C = 45° (e) Schematic diagram to provide orientation definition for 3D cubic crystal growth simulations. The different colors of crystal facets is meant for better visualization of orientation components (axial tilt and rotation axis) and is not to be confused with color-coding in preceding sub-figures.

On the basis of phase-field simulation results as shown in Figs. 2(a) - 2(f), we derive an orientation map Fig. 2(g) of crystal orientations 'A', 'B' and 'C' to establish the following selection rules:

- If every crystal has a different orientation, the crystal which is most favorably oriented (vertical in this case), survives and rest of the crystals are consumed.
- The consumption or survival of a crystal depends on its own orientation relative to its neighbors. The non-neighboring crystals do not effect the growth.
- Crystals retain the equilibrium shape (from Wulff construction) when in contact with liquid at all times.
- Crystals having the same growth orientation with respect to most preferred orientation (vertical in this case) form perpendicular grain boundaries (relative to initial surface) and co-exist in the final microstructure, if the other neighboring crystals are not more favorably oriented. This is also observed in the 3D case when two crystals have a similar orientation with respect to the vertical line but lie in different planes.

Next, we perform a 3D simulation of alum crystal growth such that crystals also develop $\{110\}$ and $\{100\}$ facets in addition to $\{111\}$ as shown in Fig. 4. Hemispherical crystal seeds are uniformly embedded at the bottom of the domain as shown in Fig. 4(a), and every crystal is assigned a random orientation with respect to the normal direction of the growth plane. The growth competition results in the consumption of poorly oriented crystals (greenish and bluish in color) and in survival of favorably oriented ones (reddish) as shown in Fig. 4(c).

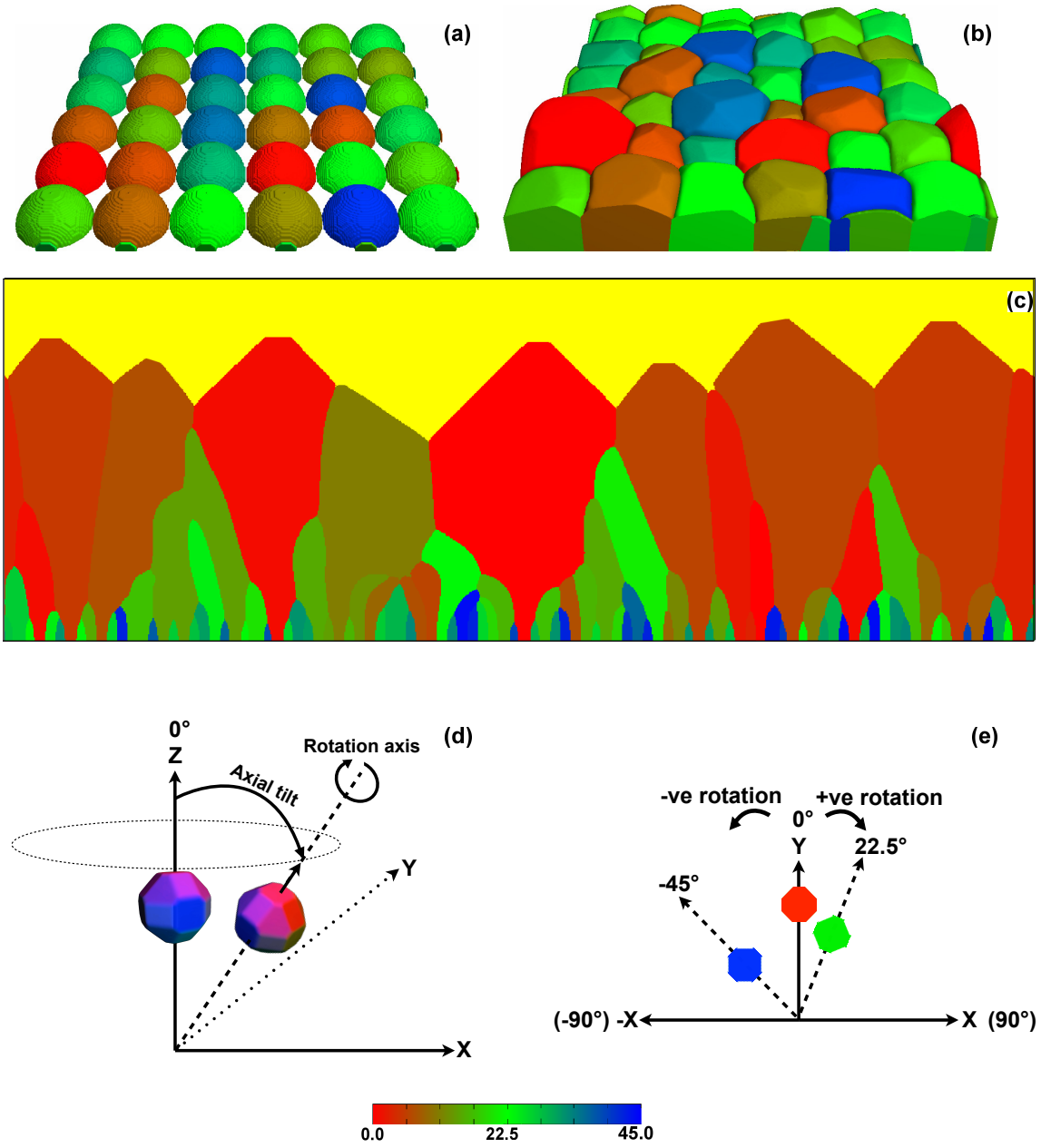

Fig. 4 Free growth of alum crystals with random orientations. (a) Bottom layer of the 3D phase-field simulation domain showing the spherical crystal nuclei and their assigned orientations in different colors. (b) intermediate stage of alum crystals growing in liquid. The facets {111}, {110} and {100} can be distinctly identified, (c) 2D simulation showing the final stage of growth competition. Favorably oriented crystals (reddish) outgrow their neighbors. (d) Orientation definitions for 3D and (e) 2D alum growth simulations. The colored crystal facets in Fig. 4(d) is provided for a better visualization and is *not* related to colorbar shown below.

4 Crack-seal growth

In the following section, we use the phase-field method described in section 2, to study the effect of various crack parameters namely roughness, opening velocity and trajectory on the crack-seal microstructure. Further, we also examine if the number of competing crystal nuclei causes a variation in the final microstructure.

Numerical simulations are carried out with periodic asperities on the crack wall and uniformly distributed crystal nuclei placed at the top of the domain. The crystals grow downwards in the direction of crack opening. All the crystals are assumed to posses a cubic anisotropy and are assigned random orientation in the range of -45° to 45° with respect to the vertical direction.

4.1 Effect of crack wall roughness

The crack surface is assumed to be periodic and the degree of roughness is controlled by the vertical angle β which is varied between 90° and 180° while keeping the wavelength constant as shown in 5(a). An angle of $\beta = 180^\circ$ corresponds to a smooth surface. The crack is opened periodically at an angle θ_{open} with respect to the vertical direction. In order to study the influence of crack roughness, we fix the value of θ_{open} to be 45°. The velocity of crack opening is selected in such a way that a complete sealing of the crack occurs before every crack opening event.

At a higher crack roughness $(\beta = 90^\circ)$, it is observed in Fig. 5(b) that the crystals track the crack opening trajectory. This is also characterized by the crack peaks (referred as 'Grain Boundary Attractor' by Hilgers et al. (2001) and Nollet et al. (2005)) attracting the grain boundaries and forcing the crystals to grow in a fibrous morphology. As the roughness angle β is successively increased in Figs. 5(c) - 5(e), the tracking behavior decreases and crystals develop curved/oscillating grain boundaries. The period of oscillation reduces with decreasing roughness.

To quantify the grain boundary tracking behavior, we plot the contour of the crystal grain boundaries (corresponding to one of the tracking grain boundary) and fit straight lines to the left and right crystal boundaries as illustrated in Fig. 5(f). The overall tracking inclination θ_{track} is defined as the mean value of the slopes of the two lines and is used to elaborate the general tracking efficiency as:

$$\mathrm{GTE} = \frac{\theta_{track}}{\theta_{open}} \tag{8}$$

The general tracking efficiency (GTE) is plotted as a function of roughness angle β in Fig. 5(g). The resulting trend indicates that the general tracking efficiency decreases for lower crack-surface roughness, beyond a certain β value. It is to be noted that the purpose of the prefix 'general' in the term 'general tracking efficiency' (GTE) is to highlight the difference with the definition of 'tracking efficiency' by Urai et al. (1991). As evident from the simulations and plotted results in Fig. 5, GTE converges to the definition of 'tracking efficiency' when crystal growth is isotropic without any oscillations. Additionally, the definition of GTE is more general as it remains valid even when characterizing the tracking behavior of oscillating grain boundaries.

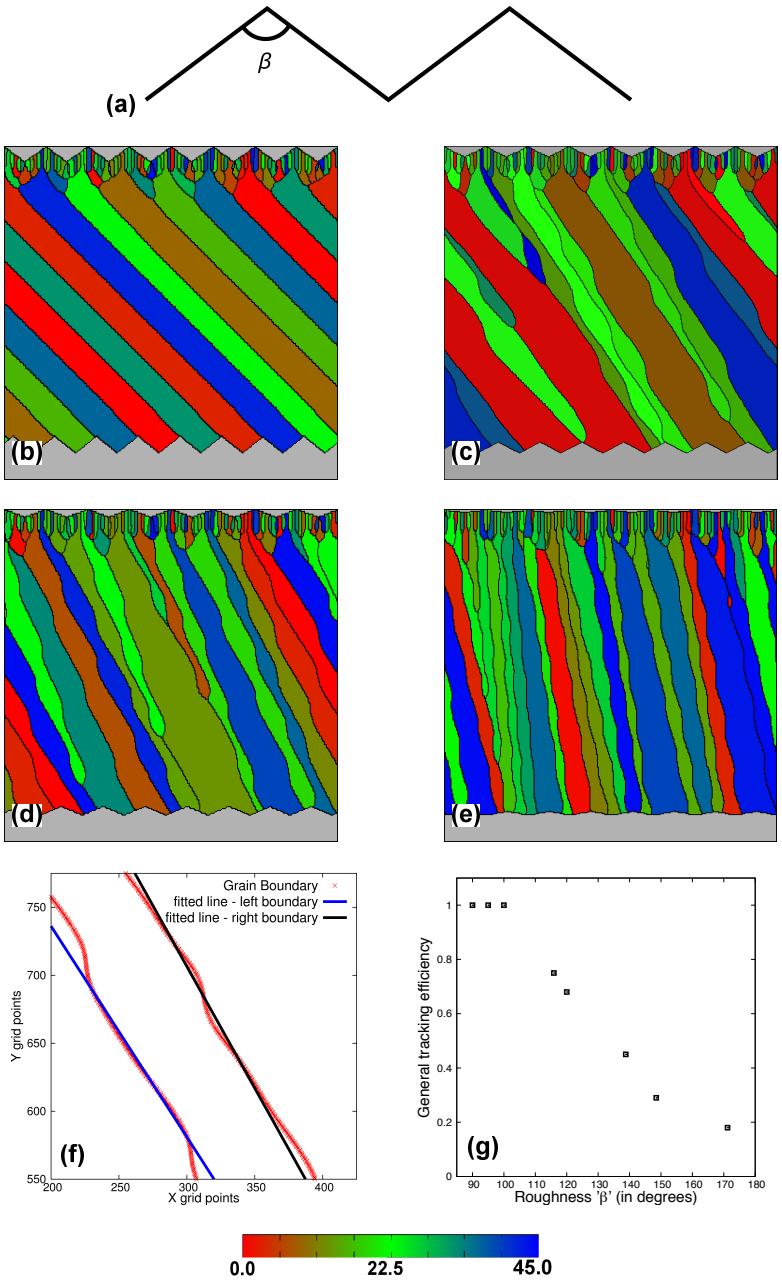

Fig. 5 Effect of crack-wall roughness on the grain boundary tracking behavior. The direction of the crack opening is θ_{open} = 45°to the vertical line. (a) The roughness of the crack is governed by angle β. The simulated grain structures refer to wall roughness of (b) 100°, (c) 120°, (d) 139° and (e) 171° (f) straight lines are fitted along the grain boundaries (g) plot of tracking efficiency as a function of crack roughness. The nature of the plot obtained from 2D phase-field simulations is consistent with the results of Urai et al. (1991). The colors refer to different crystal orientation with respect to the vertical direction (see colormap).

4.2 Effect of crack opening rate

To study the effect of crack opening velocity on vein growth, a simulation setup similar to section 4.1 is considered with 10 crystal nuclei. The roughness angle $\beta = 100^\circ$ is selected to ensure a high level of tracking efficiency, if complete sealing occurs before every opening event. The crack opening angle is kept constant ($\theta_{open} = 45^\circ$) and rate of opening is varied as shown in Fig. 6. It is observed in Fig. 6(a) that at higher crack opening rate (as compared to crystal growth rate), crystals lose contact with the crack surface. This leads to the formation of an elongate-blocky growth morphology, since crystals now grow more or less anisotropically and follow the orientation rule as observed for free-growth in Fig. 2(g). At lower crack opening rate as in Figs. 6(b) and 6(c), crystals grow isotropically in fibrous morphology, since the facet formation is suppressed. Further, within the complete crack-seal regime, at a higher opening velocity, the crystal boundaries have a tendency to curve in contrast to the case when opening velocity is smaller. The simulation results for the influence of crack opening velocity on crystal growth morphology are presented in Fig. 6. A definitive change in the crystal growth morphology is observed if crack opening rate is varied.

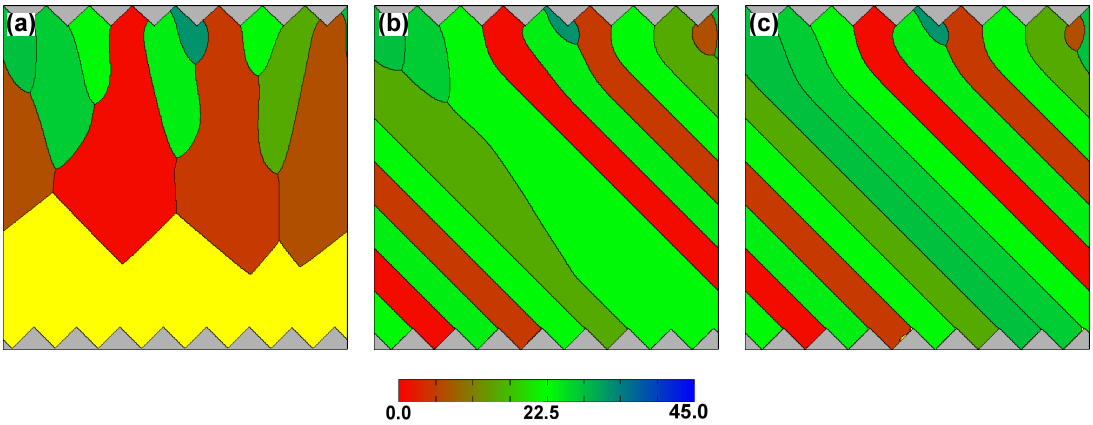

Fig. 6 Effect of crack-wall opening velocity on crystal growth morphology and final microstructure. The growth is elongate-blocky at higher crack opening rate in contrast to fibrous when the crack opening rate is slower. Further, within the complete crack seal regime, a morphological transition from curved to straight boundaries is observed. The direction of the crack opening is 45°with respect to vertical. The crack opens after every (a) 200*Δt, (b) 500*Δt and (c) 700*Δt seconds where $\Delta t = 0.12$ second refers to time-step width. The colors refer to different crystal orientation with respect to vertical (see colormap).

4.3 Effect of crack opening trajectory

In the next series of simulations, 100 crystal nuclei with different orientation are uniformly embedded at the top of the domain and the crack opening angle θ_{open} is varied. The crack roughness angle β is selected to be 100° and a complete sealing is ensured at every opening event. The phase-field simulation results show that crystals track the crack opening trajectory, irrespective of θ_{open}. Thus, the grain boundary tracking efficiency is not affected by the crack opening angle. The results of the simulation are summarized in Fig. 7. On further increasing the magnitude of the crack opening increment in Fig. 8 while ensuring complete sealing before every opening event, we observe that the tracking behavior is lost and crystals grow in a random morphology (Fig. 8(a)). However, when the crack opening increment is reduced ten-folds, while keeping θ_{open} unchanged, crystals re-establish a tracking of the crack opening trajectory as shown in Fig. 8(b).

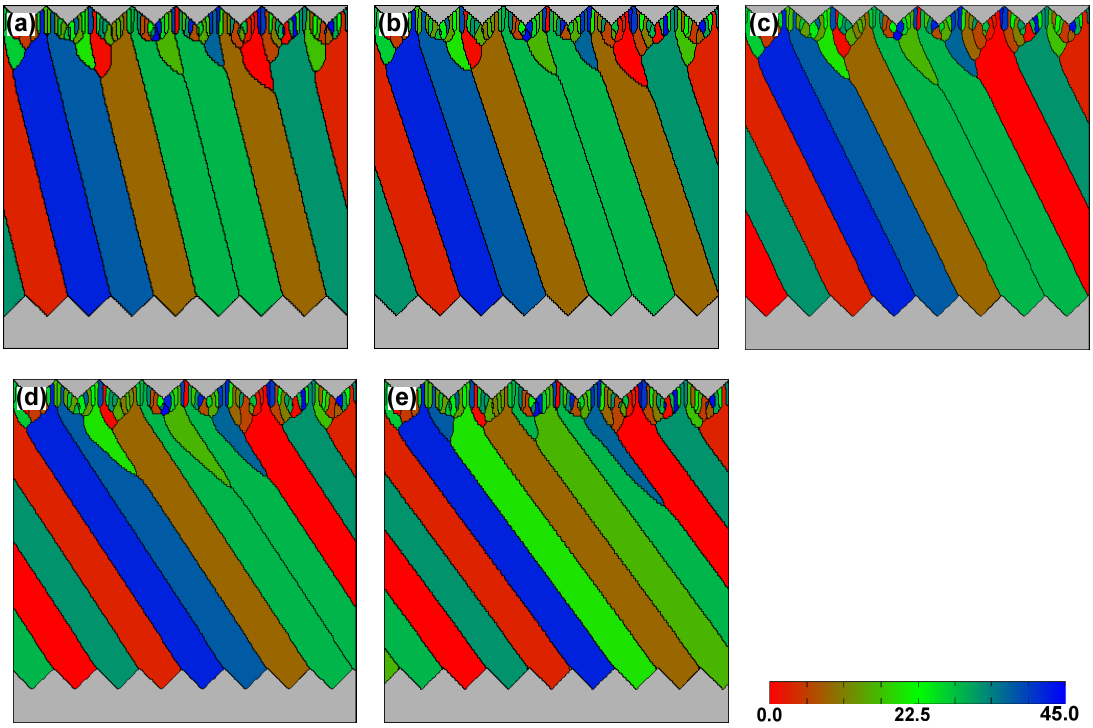

Fig. 7 Effect of crack opening trajectory on crack-seal mictrostructure. The angles of opening θ_{open} are (a) 14.0°,(b) 18.4°,(c) 26.5°,(d) 33.6°and(e) 36.8°with respect to vertical in anti-clockwise direction. The crystals track the crack opening irrespective of the trajectory, if opening increments are small and crack surface is sufficiently rough. The colors refer to different crystal orientation with respect to the vertical direction (see colormap).

4.4 Effect of number of crystal nuclei

The number of nuclei is varied to study its influence on the vein growth morphology. The crack is assumed to be sufficiently rough for 100% tracking of crystal boundaries and complete sealing is ensured. The phase-field simulations show that varying the initial number of nuclei does not influence the tracking behavior. It is noteworthy that the number of surviving crystals remains constant and is numerically equal to the number of peaks in the crack surface which faces the crystal growth front. The crystal boundaries stabilize at the crack peaks which suggest that these attract the grain boundaries. Further, we do not observe any change in growth morphology once the number of crystals surviving equals the crack peaks, irrespective of the initial number of nuclei as shown in Fig. 9. Finally, 3D phase-field simulations of crack-sealing are carried out by embedding 100 alum crystal nuclei on computationally generated rough crack surface in Figs. 10(a) and 10(b). The roughness of the 3D crack surface is controlled by varying the range of amplitude of peaks. Higher roughness relates to a wider range of maximum and minimum height of peak which is permissible (chosen randomly at different spatial locations). The crack is opened slowly to ensure ensuring complete sealing before every opening event. The 3D simulation results are displayed in Fig. 10 which shows a layer-by-layer plot of the simulation domain. The simulation results reveal that a crack surface with higher roughness forces the crystals to track the opening trajectory. As the surface roughness is reduced, the resulting grain boundaries partially form curved/oscillatory morphologies (Fig.

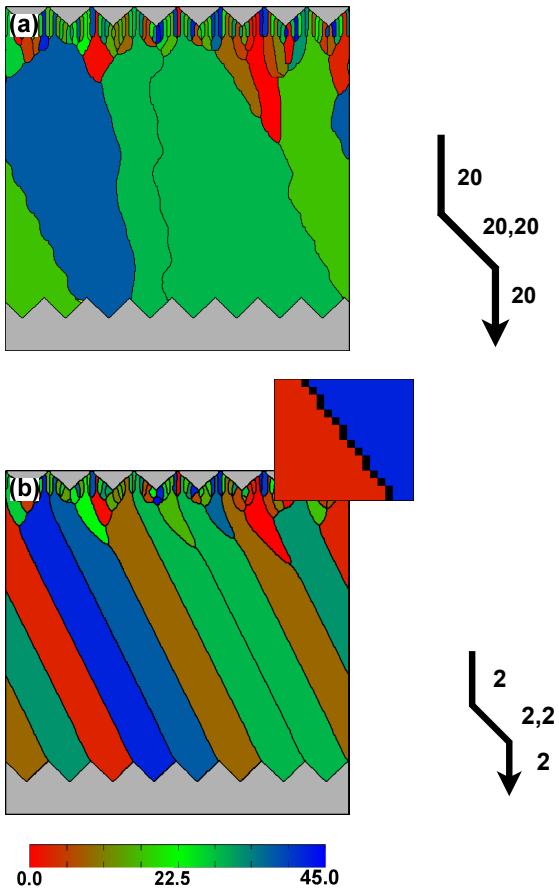

Fig. 8 Effect of crack opening increment on the crack-seal mictrostructure. The same number of crystal nuclei, crystal anisotropy and wall morphology are used as in Fig. 7. (a) Loss of tracking behavior for linear and oblique opening in large increments (20 grid-points lateral offset). (b) Grain boundary tracking for linear and oblique opening in smaller increments (2 grid-points lateral offset). Crystals track the trajectory only when opening increments are sufficiently small. The picture on upper right hand side (plot of $\phi = 0.5$) shows the grain boundary morphology provided to compare with crack-opening path. The colors refer to different crystal orientation with respect to the vertical direction (see colormap).

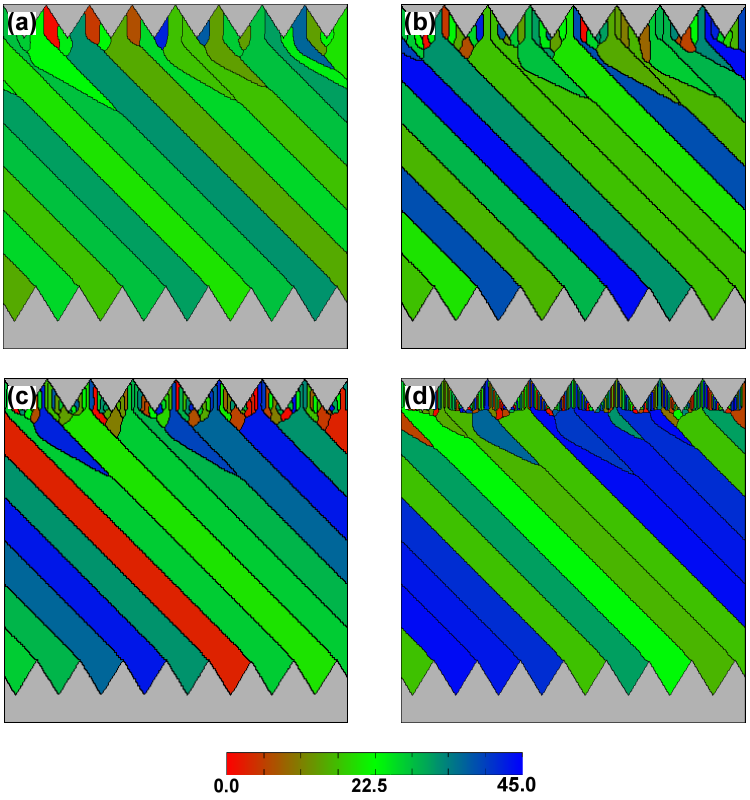

Fig. 9 Effect of initial number of nuclei on crystal growth morphology and final microstructure. The crack opening increments are small in the direction 45°with respect to vertical. The crack surface facing the crystal growth front has 8 peaks. The number of crystal nuclei are varied as in (a) 25, (b) 50, (c) 100 and (d) 250 to observe the effect on final microstructure. The number of crystals that end up tracking the crack openings is equal to the number of peaks on the advancing crack. Colors refer to different crystal orientation with respect to vertical (see colormap).

10(d)). It can be observed, that crystals grow in a mixed regime when the wall roughness is not sufficiently high.

5 Discussion of results

In the present article, the multiphase-field model for grain-growth has been extended to study the crystal growth in veins in two different growth conditions namely, free-growth in fluid and crack-sealing. In spite of considering the role of surface energy anisotropy which is responsible for crystal facet formation and growth competition, the previous algorithm for modeling vein growth (Bons, 2001) suffer from model artifacts namely 'Crystal terminations' and 'Long distance effect". The phase-field model presented in this article explains the role of surface energy anisotropy and additionally account for the interface thermodynamics and force balances at multi-grain junctions (crystal triple/quadruple points in current context). Thus, the selection dynamics of faceted crystal growth observed in the present simulations are more reliable as they compare well with the experimental findings (Hilgers and Urai, 2002a).

It is observed that the consumption or the survival of a crystal depends on its own orientation relative to neighbors, when allowed to grow freely. The non-neighboring crystals do not effect the growth of the crystal in consideration directly. Additionally, the inter-facet angle defined by the equilibrium shapes are always preserved for the crystals growing freely in liquid Figs. 1(c) and 1(d). Moreover, we do not observe any exceptions in the deduced crystal growth selection rule contrary to the findings of Nollet et al. (2005) for cubic crystal symmetry. In particular, these exceptions refer to the survival of crystals which have different orientations as well as equilibrium angle between the facets described as model artifacts. The present method is able to rectify such problems, evident from the simulations as well as orientation map and shown in Fig. 2(a) - Fig. 2(f) and Fig. 2(g) respectively. The phase-field simulation results in Figs. 2(d) and 2(e) corroborate the findings of Bons and Bons (2003) by the observation that the interface boundary between crystal 'A' and 'B' is found to be inflected. This highlights the reproducibility of previous simulation results when phase-field method is utilized. Apparently, if sufficient time is available for the development of facets, the favorably oriented crystals always out-grow the poorly oriented neighbors. We are aware of the fact that crystal growth results from an interplay of surface energy anisotropy and growth kinetics. Typically, a crystal nucleates in its equilibrium (Wulff) shape and grows asymptotically towards its "kinetic Wulff shape" if long-range transport of energy and/or mass is assumed to be extremely fast (Sekerka, 2005). Additionally, we do not rule out the possibility of different contact angles at liquid–solid triple junctions as a result of different force balances corresponding to kinetic or surface energy anisotropy. Therefore, the values of the kinetic coefficient τ and of interfacial energies need to be chosen appropriately to simulate correct selection dynamics.

The presence of a barrier for example, a rigid and rough crack surface, obstructs the freely growing crystals, forcing them to grow into a morphology unrelated to the equilibrium crystal shape. It is found that the crack parameters such as the roughness, opening velocity and trajectory determine the final crack-seal microstructure. The phase-field simulation results of crack-sealing process suggest that if the wall rock is sufficiently rough and opening velocity is small, the crystals grow isotropically, in a fibrous morphology and track the crack-opening trajectory. In this case, anisotropy in surface energy does not effect the growth morphology since facet formation is suppressed due to the additional boundary condition, which corroborates the previous simulation and experimental studies on crack-sealing process (Urai et al., 1991; Hilgers et al., 2001; Nollet et al., 2005). Moreover, higher roughness of the facing wall rock also increases the fineness of fibrous microstructure. This is inferred from Fig. 9 which shows that if the roughness is sufficiently high, the number of fibers formed is numerically consistent with the peaks on the facing crack surface. At a lower crack surface roughness, the grain boundary tracking efficiency decreases and

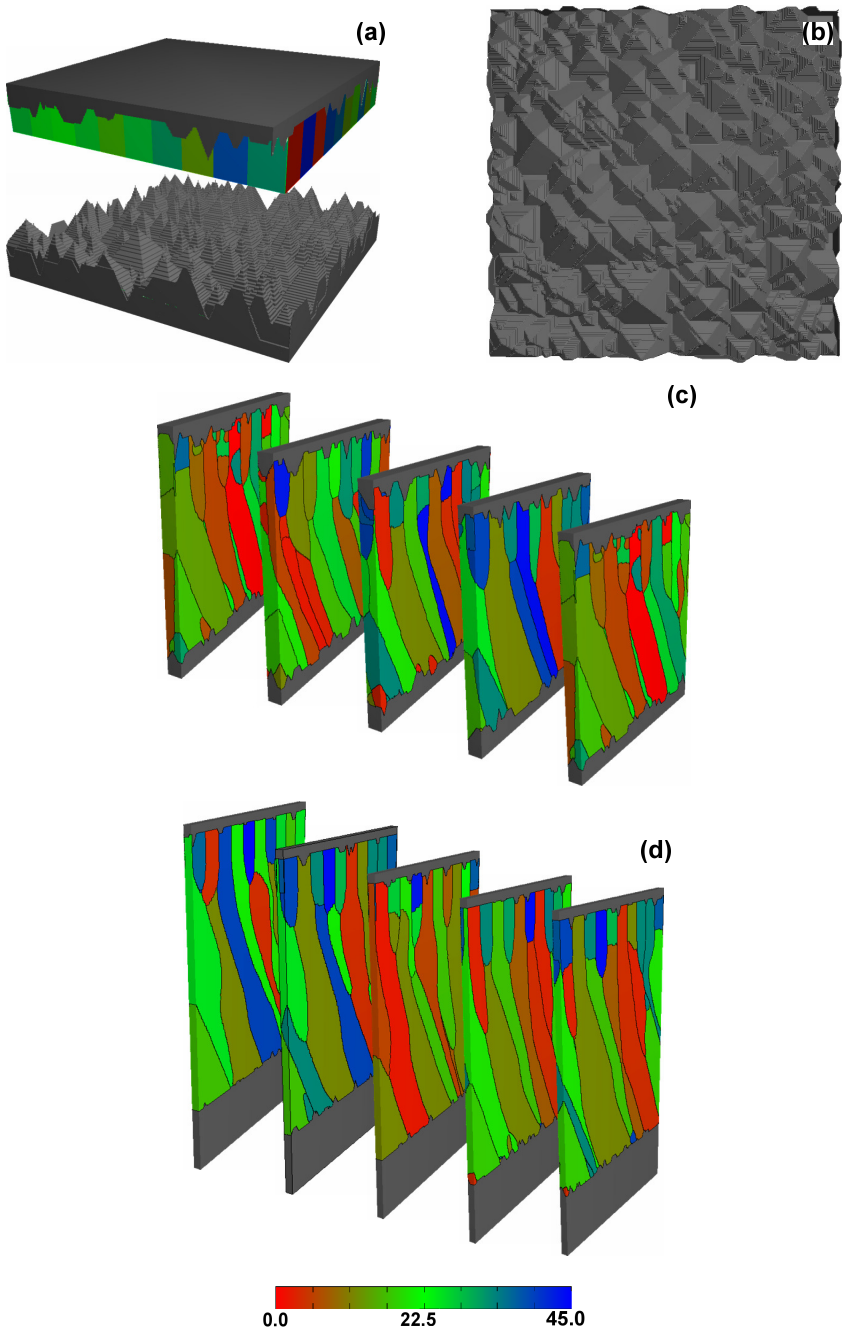

Fig. 10 Crystals are embedded on an algorithmically irregular surface for simulating crack-sealing process in 3D. The crack surface roughness is defined by the amplitude of peaks. To reduce the surface roughness, the amplitude of every peak is reduced by a numeric factor. (a) The initial simulation domain setting. (b) Top view of the crack surface. (c) 3D layer plot of the phase-field simulation of crack-sealing process showing (c) grain boundary tracking along with occasional occurrence of curved boundaries for the roughness factor 6 and for a crack opening velocity of 2 grid points lateral offset, in (d), the number of curved/inflected grain boundaries increases for the roughness factor 10 and for a crack opening velocity of 4 grid points lateral offset. The crack opening trajectory is similar to the one shown in Fig. 8(b). Colors refer to different crystal orientation with respect to vertical direction (see colormap).

the crystal boundaries have a curved/oscillating morphology as presented in Figs. 5(c), 5(d) and 5(e). The anisotropy of the surface energy provides an explanation for the curvature observed in grain boundaries in this case, as the crack opening events occur along an oblique 45° line with respect to the vertical direction. It is noteworthy, that grain boundaries alone do not provide much information about the crack-opening trajectory in such cases. The simulation results also reveal that straight grain boundaries are formed when surface energy of the growing crystals is assumed to be isotropic. Further, within the complete crack-seal regime, when the opening increment is relatively faster, curved grain boundaries are formed. The 3D phase-field study of the crack-sealing process accentuate these findings; if the wall rock roughness is low and crack opening velocity is increased while still ensuring complete sealing before every opening event, the crystals growth occurs in a mixed regime, characterized by a decrease in tracking behavior with a propensity to form curved grain boundaries. A systematic study to establish the correlation of crack roughness (by choosing more realistic boundary condition for e.g. fractal surface) and opening rate (in 3 dimensions for more relevant vein forming crystals like quartz or calcite) with the extent/amplitude of grain boundary curvature/oscillation and influence of hydrodynamic convection, is a part of on-going effort.

At this point, we would like to clarify that the objective of present work is not to question the numerical algorithm or the simulation results of Urai et al. (1991), Bons (2001), Hilgers et al. (2001) and Nollet et al. (2005). Rather, it is aimed to advance the numerical studies to 3D by adopting a thermodynamically consistent approach and to discuss the applicability of phase-field method to study polycrystal growth in veins. In this scope, the foremost intention is to discuss the reproducibility of previous results (in free-growth as well as crack-sealing 2D simulations) as well as advantages of using the present phase-field model (3D numerical studies for crystal of any shape, large-scale simulations and provision to implement transport).

6 Conclusion and outlook

In the present article, the parameters controlling the vein microstructure are studied using the phase-field method. The role of surface energy anisotropy during free growth of crystals and its influence on the grain orientation selection is addressed. The 3D phase-field simulation of free crystal growth process provides further insight on how poorly oriented crystals are consumed by more favorably oriented ones and previous ambiguities reported in literature (Nollet et al., 2005) are ruled out. Further, the influence of crack parameters on the final microstructure is discussed in detail. One of the intriguing finding of the current work is the role of surface energy anisotropy in the formation of crack-seal microstructures. Of particular importance, is the appearance of curved/oscillating crystal boundaries which draws similarities with the natural vein microstructures. The current phase-field study of crack-sealing process (in 2D and 3D) indicate that anisotropy in surface energy of the growing crystals cause the grain boundaries to curve/oscillate, if wall rock is not sufficiently rough and crack opening rate is increased gradually while still ensuring complete crack-sealing before every opening event. The fineness of the fibrous microstructure is directly related to the number of peaks on the facing wall surface. Further, the transition from fibrous to elongate-blocky morphology in vein microstructure caused by varying the crack opening rate is demonstrated in the simulation results. The present work also establishes the phase-field method as comprehensive, artifact-free and standout approach to simulate the geological processes occurring during vein formation. The simulation results also demonstrate the general capability of multiphase-field method in dealing with anisotropic 3D vein-growth problem. It is noteworthy that the numerical model presented in the current work provides a general framework to simulate crystals of any shape. Since the underlying model equations are based on continuum mechanical and thermodynamical concepts, several extensions of the present vein-growth model are possible. This includes the studies related to diffusion

driven grain evolution and hydrodynamic convection. Including such effects in the present phase-field model is imperative for the complete understanding of the vein growth problem. Once implemented, the model can be further utilized to study the precise effect of hydrodynamic convection on the morphology of the vein front and crystal boundaries. Further, this also helps in debating the question posed by Barker et al. (2006) whether vein formation involves advective fluid flow, or occurs by local diffusion of material from the surrounding wall rock. Though, this requires significant computational resources, the efficient parallelization of the phase-field solver (Nestler et al., 2008) (utilized for phase-field simulations presented in this article) makes it feasible.

7 Acknowledgements

Drs. Abhik Choudhury (Ecole Polytechnique, Palaiseau, France) and Frank Wendler (Institute of Applied Geosciences, Karlsruhe Institute of Technology) are thanked for many insightful discussions. KA and BN acknowledge the financial support by Graduate school 1483 of German Research Foundation and by the project CCMSE of the European Union (EFRE) together with the state Baden-Wuerttemberg. KA also thank former co-workers Drs. Denis Pilipenko and Michael Fleck (Materials and Process Simulations, University of Bayreuth) for preliminary discussions concerning the model and Center for Computing and Communication at RWTH Aachen University (HPC Cluster) for computational resources.

References

Barker SL, Cox SF, Eggins SM, Gagan MK (2006) Microchemical evidence for episodic growth of antitaxial veins during fracture-controlled fluid flow. Earth Planet Sc Lett 250(1–2):331 – 344

Bhat HL, Ristić RI, Sherwood JN, Shripathi T (1992) Dislocation characterization in crystals of potash alum grown by seeded solution growth under conditions of low supersaturation. J Cryst Growth 121(4):709 – 716

Bons AJ, Bons PD (2003) The development of oblique preferred orientations in zeolite films and membranes. Micropor Mesopor Mat 62(1–2):9 – 16

Bons PD (2001) Development of crystal morphology during unitaxial growth in a progressively widening vein: I. the numerical model. J Struct Geol 23(6–7):865 – 872

Bons PD, Jessell MW (1997) Experimental simulation of the formation of fibrous veins by localised dissolution-precipitation creep. Mineralogical Mag 61(1):53–63

Chen LQ (2002) Phase-field models for microstructure evolution. Annual Review of Materials Research 32(1):113–140

Cox SF, Etheridge MA (1983) Crack-seal fibre growth mechanisms and their significance in the development of oriented layer silicate microstructures. Tectonophysics 92(1–3):147 – 170

Cox SF, Etheridge MA, Wall VJ (1987) The role of fluids in syntectonic mass transport, and the localization of metamorphic vein-type ore deposists. Ore Geol Rev 2(1-3):65–86

Durney D (1972) Solution-transfer, an important geological deformation mechanism. Nature 235(5337):315–317

Durney D, Ramsay J (1973) Incremental strains measured by syntectonic crystal growths. Gravity and Tectonics pp 67–96

Durney DW (1976) Pressure-solution and crystallization deformation. Phil Trans R Soc A 283(1312):229–240

Fisher DM, Brantley SL (1992) Models of quartz overgrowth and vein formation: deformation and episodic fluid flow in an ancient subduction zone. J Geophys Res 97(B13):20,043–20,061

Hilgers C, Urai JL (2002a) Experimental study of syntaxial vein growth during lateral fluid flow in transmitted light: first results. J Struct Geol 24(6–7):1029 – 1043

Hilgers C, Urai JL (2002b) Microstructural observations on natural syntectonic fibrous veins: implications for the growth process. Tectonophysics 352(3–4):257 – 274

Hilgers C, Koehn D, Bons PD, Urai JL (2001) Development of crystal morphology during unitaxial growth in a progressively widening vein: II. Numerical simulations of the evolution of antitaxial fibrous veins. J Struct Geol 23(6–7):873 – 885

Kim SG, Kim DI, Kim WT, Park YB (2006) Computer simulations of two-dimensional and three-dimensional ideal grain growth. Phys Rev E 74:061,605

Klapper H, Becker RA, Schmiemann D, Faber A (2002) Growth-sector boundaries and growth-rate dispersion in potassium alum crystals. Cryst Res Technol 37(7):747–757

Knipe RJ, McCaig AM (1994) Geofluids: origin, migration and evolution of fluids in sedimentary basins, pp 99–111

Koehn D, Hilgers C, Bons PD, Passchier CW (2000) Numerical simulation of fibre growth in antitaxial strain fringes. J Struct Geol 22(9):1311 – 1324

McCaig AM (1988) Deep fluid circulation in fault zones. Geology 16(10):867–870

Mügge O (1925) Über gehemmtes kristallwachstum. Z Kristallogr 62(5/6):415–442

Mullin JW (2001) Crystallization. Butterworth-Heinemann, Oxford

Nestler B, Choudhury A (2011) Phase-field modeling of multi-component systems. Current Opinion in Solid State and Materials Science 15(3):93 – 105

Nestler B, Garcke H, Stinner B (2005) Multicomponent alloy solidification: Phase-field modeling and simulations. Phys Rev E 71:041,609

Nestler B, Reichardt M, Selzer M (2008) Massive multi-phase-field simulations: methods to compute large grain system. In: Hirsch J, Skrotzki B, Gottstein G (eds) Proceedings of the 11th International Conference on Aluminium Alloys, Aachen, Germany, pp 1251–1255

Nollet S, Urai JL, Bons PD, Hilgers C (2005) Numerical simulations of polycrystal growth in veins. J Struct Geol 27(2):217 – 230

Nollet S, Hilgers C, Urai JL (2006) Experimental study of polycrystal growth from an advecting supersaturated fluid in a model fracture. Geofluids 6(2):185–200

Ramsay JG (1980) The crack-seal mechanism of rock deformation. Nature 284(5752):135–139

Ramsay JG, Huber MI (1983) The Techniques of Modern Structural Geology: Strain analysis, The Techniques of Modern Structural Geology, vol 2, Academic Press, pp 185,192

Schmidegg O (1928) Über geregeltes wachstumsgefüge. Jb Geol Bundesanstalt 78:1–51

Sekerka RF (2005) Equilibrium and growth shapes of crystals: how do they differ and why should we care? Cryst Res Technol 40(4-5):291–306

Singer-Loginova I, Singer H (2008) The phase field technique for modeling multiphase materials. Reports on Progress in Physics 71(10):106,501

Stinner B, Nestler B, Garcke H (2004) A diffuse interface model for alloys with multiple components and phases. SIAM J Appl Math 64(3):775–799

Thijssen JM, Knops HJF, Dammers AJ (1992) Dynamic scaling in polycrystalline growth. Phys Rev B 45:8650–8656

Thornton K, Ågren J, Voorhees P (2003) Modelling the evolution of phase boundaries in solids at the meso- and nano-scales. Acta Materialia 51(19):5675 – 5710

Urai JL, Williams PF, van Roermund HLM (1991) Kinematics of crystal growth in syntectonic fibrous veins. J Struct Geol 13(7):823 – 836

Williams PF, Urai JL (1989) Curved vein fibres: an alternative explanation. Tectonophysics 158(1–4):311 – 333

Yardley BWD, Jamtveit B (1997) Fluid flow and transport in rocks : mechanisms and effects. Chapman & Hall, London

Zhang J, Adams JB (2002) Facet: a novel model of simulation and visualization of polycrystalline thin film growth. Model Sinul Mater Sc 10(4):381